AGU PUBLICATIONS

Global Biogeochemical Cycles

RESEARCH ARTICLE
10.1002/2013GB004797

Key Points:
- Twenty-two year series of group phytoplankton carbon reconstructed for Sargasso Sea
- Increasing trend in total carbon and phase shifts in community structure
- Trend/shifts likely due to varying frequency/seasonality of vertical mixing

Supporting Information:
- Readme
- Text S1–S7 and Figures S1–S12
- Table S1
- Table S2
- Table S3
- Table S4
- Table S5

Correspondence to:
P. J. Wallhead,
philip.wallhead@niva.no

Citation:
Wallhead, P. J., V. C. Garçon, J. R. Casey, and M. W. Lomas (2014), Long-term variability of phytoplankton carbon biomass in the Sargasso Sea, *Global Biogeochem. Cycles*, *28*, 825–841, doi:10.1002/2013GB004797.

Received 17 DEC 2013
Accepted 22 JUL 2014
Accepted article online 26 JUL 2014
Published online 12 AUG 2014

Long-term variability of phytoplankton carbon biomass in the Sargasso Sea

Philip J. Wallhead[1,2], Véronique C. Garçon[2], John R. Casey[3], and Michael W. Lomas[4]

[1]Now at Norwegian Institute for Water Research, Bergen, Norway, [2]Laboratoire d'Etudes en Géophysique et Océanographie Spatiales, Toulouse, France, [3]Center for Microbial Oceanography: Research and Education, School of Ocean and Earth Science and Technology, University of Hawai'i at Mānoa, Honolulu, Hawaii, USA, [4]Bigelow Laboratory for Ocean Sciences, East Boothbay, Maine, USA

Abstract Time series of phytoplankton carbon biomass are scarce yet may provide important insights into ocean productivity and carbon export to depth via the oceanic biological pump. We combine recent flow-cytometric measurements with pigment concentrations and other standard measurements to reconstruct taxon-specific phytoplankton carbon biomass in the Sargasso Sea over 22 years, using a multiple regression approach. The reconstructed series reveal an increasing trend (~3% per year) in total phytoplankton carbon, apparently driven by increasing nutrient supply by vertical mixing associated with a shift to a negative phase in the winter North Atlantic Oscillation index. Also, the reconstructed eukaryote biomass fraction shows a multiannual shift from ~45% in the early 1990s/late 2000s to ~70% in the late 1990s/early 2000s. We hypothesize that a multiannual shift in the seasonal pattern of mixing may have stimulated and restructured the eukaryote community while suppressing prokaryote populations by increasing photodamage and grazing mortality.

1. Introduction

The carbon biomass of marine phytoplankton plays a key role in determining the available food for higher trophic levels, the carbon export by sinking particles, and the primary productivity of the world's oceans [*Geider et al.*, 1998; *Behrenfeld et al.*, 2005; *Westberry et al.*, 2008]. Yet it is only in recent years that efficient methods have been developed to measure phytoplankton carbon by flow cytometry [*Veldhuis and Kraay*, 2000; *DuRand et al.*, 2001; *Worden et al.*, 2004; *Graff et al.*, 2012; *Casey et al.*, 2013]. Measured chlorophyll *a* (chl *a*) concentrations have traditionally been converted to carbon biomass using empirical formulae [e.g., *Cloern et al.*, 1995], but these tend to imply large uncertainties due to taxonomic variability and difficulties in predicting nutritional and photoadaptive state. Long-term ocean time series for phytoplankton carbon biomass therefore remain scarce, compromising efforts to understand the effects of climatic variability on ocean biogeochemical cycles and to develop predictive models. There is also an increasing demand for biomass data that is resolved into groups, such as size classes or functional types, in order to ground truth remote sensing estimates and to better understand and model processes, such as primary production, that may strongly depend on the structure of the phytoplankton community.

The Bermuda Atlantic Time-series Study (BATS) is a long-term sampling program located in the western North Atlantic subtropical gyre or Sargasso Sea (see *Lomas et al.* [2013] for a recent review). It has generated an unusually complete and long-term (24 year) open-ocean data set and is consequently a key resource for investigating seasonal and longer-term biogeochemical dynamics in the subtropical gyres (the world's largest ecosystems covering >40% of the Earth's surface) and for developing and assessing large-scale biogeochemical models and satellite algorithms [e.g., *Saba et al.*, 2010]. That said, the BATS time series are likely still too short to reflect anthropogenic climate changes in ocean primary productivity and biomass, due to the relatively strong interannual and multiannual/decadal variability in these quantities [*Martinez et al.*, 2009; *Boyce et al.*, 2010, 2012; *Henson et al.*, 2010], as does not appear to be the case for pCO_2 and carbonate chemistry parameters [*Bates*, 2012; *Bates et al.*, 2012].

In this study we combine recent flow-cytometric data with BATS "core" variables and a multiple regression model to reconstruct taxon-specific phytoplankton carbon over the entire BATS record. We then attempt to explain the reconstructed biomass variability as a product of biogeochemical/ecosystem processes, focusing on nutrient supply, mixing-induced light shock, and possibly-mixotrophic grazing. The reconstruction confirms a 22 year increasing trend in total phytoplankton biomass [*Lomas et al.*, 2010a] and also reveals multiannual

variations in phytoplankton community structure, comparable to those observed in the North Pacific subtropical gyre [*Corno et al.*, 2007] but smoother and less dramatic than the "regime shifts" observed in the Caribbean Sea [*Taylor et al.*, 2012]. Our results challenge traditional assumptions that link enhanced eukaryotic algal biomass with enhanced nutrient supply and provide empirical constraints on long-term phytoplankton biomass variability which are critically needed to develop and validate large-scale biogeochemical models.

2. Methods

2.1. Data Preprocessing

We obtained flow-cytometric phytoplankton carbon data from J. Casey [*Casey et al.*, 2013] and raw data for BATS core variables from the project website (http://bats.bios.edu). Group-resolved phytoplankton carbon was calculated from flow-cytometric estimates of cell abundance for each group and carbon per cell derived from forward light scatter [see *Casey et al.*, 2013]. Mixed layer depths (MLDs) were derived from the BATS conductivity-temperature-depth data (2 m resolution) using a variable σ_t criterion, where σ_t is the seawater density (kg m^{-3}) referenced to atmospheric pressure without temperature adjustment [*Sprintall and Tomczak*, 1992; *Steinberg et al.*, 2001; *Lomas et al.*, 2013]. After inspecting a large number of individual profiles, we decided that a $\Delta\sigma_t$ equivalent to 0.2°C temperature drop relative to 10 m depth values gave reasonable MLDs, mostly including the remnant layer of diel mixing and avoiding diurnal stratification effects [*Brainerd and Gregg*, 1995]. Only data shallower than 275 m and within a radius of 0.3° from the nominal BATS location (64.17°N, 31.67°W) were considered in our analyses. Zero values for nonnegative variables (such as pigments) were replaced with the minimum-observed nonzero value in order to avoid problems with transformations (see below).

The raw data were first block averaged onto a depth-time grid with 12 nominal depths: (1, 10, 20, 40,…, 160, 200, and 250) m and nominal times at the centers of seasonal windows: "Winter" = January-February-March, "Spring" = April-May-June, "Summer" = July-August-September, and "Fall" = October-November-December. This gridding serves to (1) facilitate the matchup between core and phytoplankton carbon variables, (2) allow standard errors (SEs) for the data to be estimated from the "replicate" measurements within each block, (3) promote the normality of the data (by the Central Limit Theorem), (4) simplify the autocorrelation structure of the time series, and (5) reduce the tendency to confuse temporal variations with advected spatial variations in the sampled region. SEs were estimated by smoothing the variance estimates from individual blocks as a function of the block mean (Gaussian kernel, half width = 0.2 × the range of mean values) then taking $\mathrm{SE} = n^{-1/2}\hat{\sigma}$, where $\hat{\sigma}^2$ is the smoothed variance and n is the number of replicates (usually $n = 3$–6, including one sample close to the nominal depth per cruise, with 15–30 days between cruises). This does neglect correlation between replicates but also neglects finite block extent and systematic variation within blocks and generally gave reasonable SEs. For MLD and temperature, multiple profiles were sampled during each cruise; hence, raw data were preaveraged onto months (and if necessary grid depths) to ensure conservative SEs.

2.2. Time Series Analysis

To limit the number of analyses, we mostly consider time series of averages over seasons and a fixed "euphotic" depth of 140 m, a ~0.1% light level [*Siegel et al.*, 2001] that includes ~90% of the total phytoplankton biomass [*Casey et al.*, 2013]. These were estimated by trapezoidal integration of the gridded data, by default allowing up to 35 m extrapolation of the shallowest/deepest value toward the upper/lower limit (otherwise excluding the profile). SEs were estimated by treating the subseasonal vertical averages as replicates and applying the above smoothing method.

Long-term variability was first analyzed "nonparametrically" by applying a 3 year running mean to the data series $y(t)$. SEs for the 3 year means were propagated from the seasonal data SEs assuming independent (but unequal variance) errors, and confidence intervals (CIs) were constructed via a normal approximation. The 3 year means were extended to the limits of the series, neglecting boundary bias [*Hastie et al.*, 2009]. Second, the series were analyzed parametrically by fitting the model:

$$y'_i = \beta_0 + \beta_1 t_i + \delta(\beta_{2-4}, t_i) + \varepsilon_i \quad (1)$$

where the prime denotes a Box-Cox transformation with parameter λ: $y' = \lambda^{-1}(y^{\lambda} - 1)$ [*Box and Cox*, 1964]. A suitable power transformation was thus determined from the data ($\lambda = 0$ gives a log transform). The parameter β_1 describes the long-term trend, and β_{2-4} are seasonal contrast parameters (3 degrees of freedom, allowing all possible variations in seasonal means that are cyclical and zero sum over four seasons). The remaining

variability is modeled as a first-order autoregressive (AR1) process: $\varepsilon \sim N(0, C)$ where $C_{ij} = \sigma_\varepsilon^2 \rho^{h^{-1}|t_i - t_j|}$, with autocorrelation parameter ρ and step size $h = 0.25$ years. Parameters were fitted jointly by maximum likelihood estimation with the usual neglect of the implicit truncation in the distribution of ε [*Abrevaya*, 2002] and applying the [*Doran et al.*, 1992] bias correction for $\hat{\rho}$ (see Text S1 in the supporting information). Tests of model adequacy were performed on the fit residuals after prewhitening to remove the AR1 correlation, using the Cholesky decomposition of $\hat{C}^{-1}$, and studentizing to remove the effects of fitted parameters on homogeneity of variance [*Montgomery et al.*, 2012]. Tests of normality (Lilliefors), independence (Ljung-Box), and homogeneity of variance (Koenker-Bassett) seldom flagged a significant lack of fit. CIs for $\{\lambda, \rho\}$ were computed using the Fisher information and a normal approximation (this gave close-to-nominal coverage in simulations; see Text S2). In many cases the CIs for λ excluded zero or one half, thus rejecting the simpler log and square root transforms; usually, the lower CI limits for ρ were > 0 and Durbin-Watson tests on residuals from fits assuming $\rho = 0$ rejected the no-autocorrelation model.

Trend significance was tested by a t test of the hypothesis $\beta_1 = 0$, using $\hat{C}^{-1}$ to compute SEs (this gave accurate Type I error rates in simulations; see Text S1). To measure the trend on the original scale, we define the "trend increase" T as the % difference between expected annual means in 1990 versus 2010, normalizing by the 1990 value. These means were averages of seasonal expected values, estimated by integrating the fitted distribution of y (Text S3; note that this fit includes all the available data from 1989 through 2011/2012). Analysis of the reconstructed data suggested the addition of a "multiannual shift" effect to measure variability associated with the reconstructed phase shifts in community structure. We therefore added to equation (1) a "smoothed top-hat" effect $f(t) = \beta_5 \left(\tanh \frac{(t-t_1)}{\tau} + \tanh \frac{-(t-t_2)}{\tau} \right)$, where $(t_1, t_2) = (1997.5, 2005.5)$ years, $\tau = 1$ year, and β_5 is an additional free parameter. The multiannual shift S was then defined as the % difference between expected annual means in 1990 versus 2001, excluding trend effects (centered on 2001) and normalizing by the 1990 value. CIs for (T, S) were derived by a Monte Carlo method that gave close-to-nominal coverage in simulations (Text S2).

2.3. Data Reconstruction

For phytoplankton carbon (mg C m^{-3}), analysis of long-term variability was restricted by the fact that regular measurements have only been made since 2004. We attempt to lift this restriction by predicting group phytoplankton carbon from BATS "core" variables that have been sampled since 1989. As predictors we use all regularly sampled high-performance liquid chromatography (HPLC) pigments (ng/kg; see Table S3) as these inform about the relative abundance and taxonomic composition of the phytoplankton. Dissolved concentrations (μmol/kg) of nitrate-plus-nitrite N + N and soluble reactive phosphate "PO_4" were included as Sargasso Sea phytoplankton are thought to be mainly nitrogen limited [*Lipschultz et al.*, 2002; *Glover et al.*, 2007], with phosphorus playing a secondary role [*Lomas et al.*, 2004, 2010b; *Moore et al.*, 2008] (note that long-term ammonium time series were not available, and autoanalyzer data were used in lieu of sufficiently complete series from more sensitive methods [*Lipschultz*, 2001; *Lomas et al.*, 2010b]). Particulate organic carbon and nitrogen (POC and PON, μg/kg) were used as phytoplankton biomass is a component of these values, and they inform about cellular nutrient status, which also affects the cellular carbon : chl ratio. Water temperature T (°C) and in situ photosynthetically active radiation (PAR) (Ein m^{-2} d^{-1}) are also known to affect cell stoichiometry via physiological and genetic adaptation. PAR was estimated using astronomical formulae, a simple cloud transmission model, and a log linear profile model for attenuation (Text S4). Estimates within the mixed layer were averaged over the mixed layer to give the daily average PAR experienced by mixing cells.

The gridded predictor variables were first normalized via a simple Box-Cox pretransform; this tended to improve predictive potential and the performance of the hat matrix criterion (see below; no transform was deemed necessary for T). The predictors were also standardized (subtracting the sample mean and dividing by the standard deviation) to facilitate a ranking of their impact on the response. We then fitted by maximum likelihood the model

$$y_i' = b_0 + \sum_{j=1}^{m} b_j \bar{x}_{ij} + \eta_i \tag{2}$$

where y' is the Box-Cox transform of the gridded phytoplankton carbon data ($n = 358$), $\bar{x}$ are the standardized predictors ($m = 20$), and $\eta \sim N\left(0, \sigma_\eta^2\right)$. Plots of residuals versus $\bar{x}$ values showed no obvious evidence of

neglected nonlinearity. The model was applied to predict gridded phytoplankton carbon data from fall 1989 through fall 2011, using the unbiased back transform (Text S3). SEs in grid predictions were calculated by a parametric bootstrap technique that accounted for the error correlation formally neglected in equation (2) (Text S5), and CIs for 3 year means were derived from percentiles of the bootstrap ensemble of depth and time averages. The reconstructed series were then analyzed as described above, treating the predictions as unbiased data in equation (1). To calculate euphotic averages, we considered it safe to raise the maximum allowed extrapolation toward the surface to 45 m, allowing one extra datum in winter 2001 when the average MLD was 101 m.

Given the number of predictors, and the fact that several are somewhat correlated, equation (2) is unlikely to be a robust extrapolator. This was not a severe limitation, however, because the prediction problem was largely interpolative, with only ~5% of grid prediction points classed as extrapolations by the hat matrix criterion [*Montgomery et al.*, 2012]. As a safeguard, these extrapolation points were excluded from all subsequent analyses. We also considered the use of model selection to obtain a more robust predictive model [e.g., *Burnham and Anderson*, 2002]. A simple stepwise regression algorithm was able to improve Akaike's Information Criterion and the Bayesian Information Criterion by reducing m to 8–12; however, this did not generally improve the cross-validation skill (skill in predicting profiles withheld from the fit) when the variability in selected subsets was accounted for (Table S4), and the model selection did not always reduce the number of extrapolation points. In any case, very similar trends and multiannual shifts were obtained whether or not model selection was applied and whether or not the extrapolation points were excluded (Figures S11 and S12). We attribute this insensitivity to the interpolative nature of the predictions and the subsequent averaging of prediction errors over depth and time.

2.4. Explanatory Analyses

In order to explain the reconstructed variability, we consider various "biomass" and "explanatory" variables, as averages over seasons and (where applicable) the euphotic depth. Biomass variables include chlorophyll *a* (ChlA, ng/kg), primary productivity (PP, mg C m^{-3} d^{-1}), and phytoplankton carbon as measured by the original data (PC, etc.) and by the reconstructed data (PCr, etc.). Explanatory variables focus on nutrient supply, light shock, and grazing pressure as potential causal mechanisms. Dissolved nutrient concentrations (N + N, PO_4) are generally expected to increase with nutrient supply rates, though this may be counteracted by the stimulation of biological uptake. The molar ratio POC : PON (POCN) should increase with increasing N limitation at the community level [e.g., *Karl et al.*, 2001] (we present averaged ratios, but ratios of averages gave very similar results; particulate phosphorus series were too short to allow long-term POCP analysis). Heat content (T) should decrease with increasing vertical exchange (whether by convective overturn, small-scale "diffusive" mixing or eddy/submesoscale advection), and hence decrease with increasing nutrient supply. Surface wind speed WS (m s^{-1}, measured at Bermuda Airport) should correlate positively with nutrient supply by vertical mixing [*Marra et al.*, 1990] and eddy-wind interactions [*McGillicuddy et al.*, 2007; *Mahadevan et al.*, 2008]. Mixed layer depth as defined above (MLD_1) should reflect the intensity of the deepest mixing events (convective overturn), and hence both nutrient supply and light variability. We also consider a 0.02°C variable-σ_t criterion relative to 2.5 m depth ($MLD_2 \approx$ mixing layer depth [*Brainerd and Gregg*, 1995]) which should reflect the intensity of near-surface diurnal mixing. As further measures of vertical exchange/nutrient supply, we consider the density stratification index $\Delta\rho \equiv \rho_{200} - \rho_0$ (kg m^{-3}) [*Behrenfeld et al.*, 2006; *Lozier et al.*, 2011] and the seasonal North Atlantic Oscillation (NAO) index of *Hurrell and Deser* [2009]. This latter measures a mode of climate variability in the Northern Hemisphere that influences the frequency of winter storm arrival at the BATS site [*Bates*, 2001; *Lomas et al.*, 2010a; *Casey et al.*, 2013]. Finally, the total mesozooplankton biomass Z (>200 μm, units mg C m^{-3}) is considered as a measure of grazing pressure, acknowledging that our analyses are limited by the lack of regular biomass or grazing rate data for nanozooplankton/microzooplankton [*Lessard and Murrell*, 1998]. To limit the effect of outliers, truly exceptional N + N data for 2010 and 2011 (Figure S5q) were excluded from the analyses. Lack-of-fit tests suggested that the time series model was reasonable for most variables except $MLD_{1,2}$ which failed the Koenker-Bassett test ($p < 10^{-3}$) due to strong seasonality in the residual variance; this was remedied by replacing the Box-Cox transform with a pretransform to seasonal z-scores for $MLD_{1,2}$ [*Corno et al.*, 2007].

Time series models were first fitted to the biomass and explanatory variables, including the multiannual shift as well as the seasonal and trend effects. We then investigated year-to-year interannual variability by

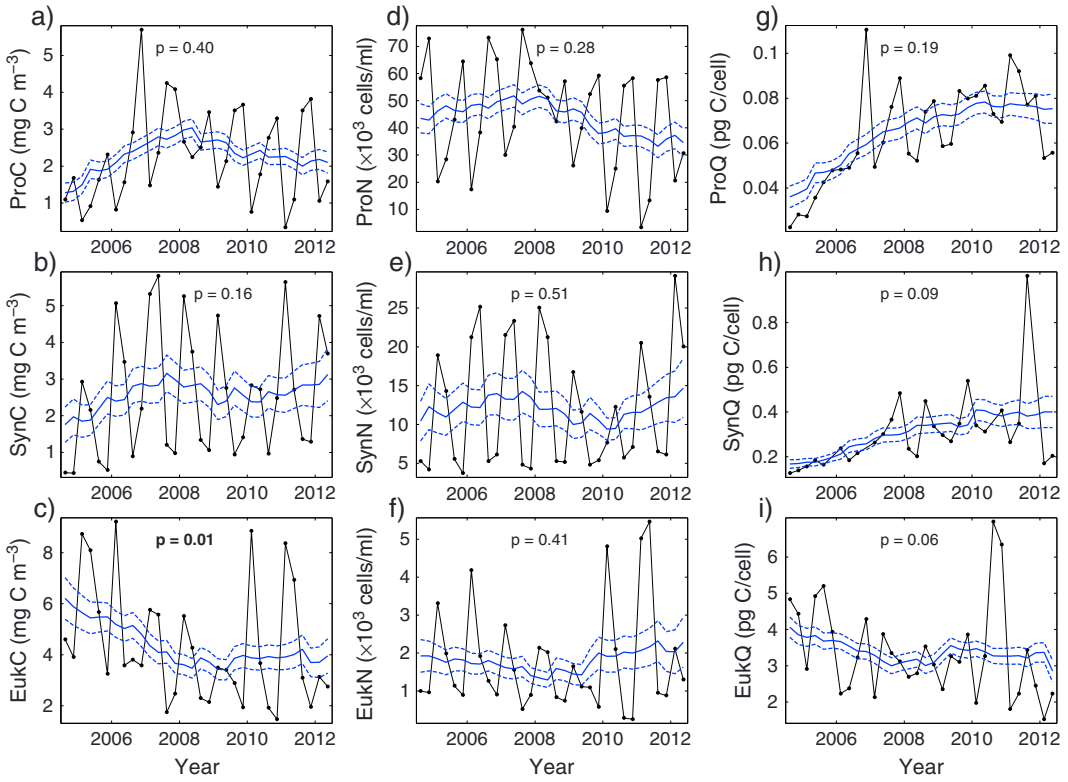

Figure 1. Time series of group phytoplankton data for (a, d, g) *Prochlorococcus*, (b, e, h) *Synechococcus*, and (c, f, i) eukaryote groups in terms of carbon concentration (Figures 1a–1c), cell numbers (Figures 1d–1f), and carbon (Figures 1g–1i): cell, showing seasonal and 0–140 m average data (black dots) and 3 year running means (blue lines, envelopes are 95% CIs derived from the subseasonal sampling variance). *P* values are for the trend significance (bold < 0.05).

testing zero-lag Pearson cross correlations between the fit residuals for biomass and explanatory variables. These residuals were studentized and prewhitened to avoid exaggerated significance due to neglected autocorrelation [*Chatfield*, 1975] (similar results were obtained using the corrected degrees of freedom method of *Pyper and Peterman* [1998]). Shift and trend effects were then tested for significance via *t* tests of the hypotheses $\beta_5 = 0$ and $\beta_1 = 0$, respectively, and CIs were computed for *S* and *T*. Analyses were repeated for individual seasons by subsetting residuals or, for the shift and trend variability, by refitting the model without seasonal effects to single-season subsets of the data. For these latter fits, where $n \sim 22$, simulations suggested that ρ may be poorly constrained and the bias undercorrected, yielding somewhat unconservative *t* tests and CIs at high true values of ρ (Figures S1 and S2). However, similar application results were obtained with the autocorrelation neglected (setting $\rho = 0$), and subsequent Durbin-Watson tests rarely cast doubt on the significant effects.

3. Results and Discussion

3.1. Analysis of the Original Time Series

In terms of 3 year means, the original phytoplankton carbon data show significant increases since 2004 in *Prochlorococcus* and *Synechococcus* carbon (ProC and SynC, Figures 1a and 1b) and a decrease in eukaryote (algal) carbon (EukC, Figure 1c), a heterogeneous group thought to consist largely of prasinophytes, pelagophytes, and haptophytes [*Lomas and Bates*, 2004]. The biomass variability appears to result less from changes in cell numbers (Figures 1d–1f) than from changes in carbon per cell (Figures 1g–1i), which for the prokaryote groups has roughly doubled since 2004. Fitting the time series model with seasonal and trend effects reveals a significant decrease in EukC (Figure 1c), but otherwise the shortness and autocorrelation of these series prohibit trend significance. Significant trends are, however, identifiable in the biomass predictor variable time series, which are over 3 times as long (Text S6).

Table 1. Data Reconstruction Models for Phytoplankton Carbon[a]

Model	ME	ME $\langle\rangle_z$	ME_{cv} $\langle\rangle_z$	$\%E_{cv}$ $\langle\rangle_z$	Significant Predictors
PCr	0.90	0.82	0.68	17	$Diad^{(+)}$, $PAR^{(+)}$, $N+N^{(-)}$, $Peri^{(+)}$
ProCr	0.79	0.72	0.53	37	$ZeaL^{(+)}$, $ChlB^{(+)}$, $BFuc^{(+)}$, $T^{(+)}$, $Allo^{(-)}$, $Diad^{(-)}$, $PO_4^{(+)}$, $ABC^{(+)}$, $Diat^{(-)}$
SynCr	0.76	0.78	0.48	50	$ChlA^{(+)}$, $ChlB^{(-)}$, $C12^{(-)}$, $PAR^{(+)}$, $Diad^{(+)}$, $N+N^{(-)}$, $T^{(-)}$, $Allo^{(+)}$, $PON^{(+)}$
EukCr	0.81	0.82	0.66	31	$C12^{(+)}$, $BFuc^{(+)}$, $PAR^{(+)}$, $Diad^{(+)}$, $ZeaL^{(-)}$, $PO_4^{(-)}$, $ChlB^{(+)}$, $Peri^{(+)}$, $Allo^{(+)}$

[a]ME is the modeling efficiency or general R^2 value (ME = 1 − SSR/SSD with SSR the sum-of-squared residuals and SSD/(n − 1) the sample variance on the untransformed scale). ME $\langle\rangle_z$ is the modeling efficiency with respect to euphotic averages (0–140 m), and ME_{cv} $\langle\rangle_z$ is the same efficiency with respect to cross-validation data (aggregating over 30 leave-one-profile-out cross validations). $\%E_{cv}$ $\langle\rangle_z$ is the root-mean-square error (on the untransformed scale) between predicted and cross-validation euphotic averages, as a % of the sample mean. Significant predictors are regressor variables with coefficients significant at the 95% level (bootstrap test, Text S5), in order of decreasing impact on the response, with superscripts denoting the sign of the effect. C3 = chlorophyll c_3, C12 = chlorophylls $c_1 + c_2$, Peri = peridinin, BFuc = 19′-butanoyloxyfucoxanthin, Fuco = fucoxanthin, Diad = diadinoxanthin, Diat = diatoxanthin, Allo = alloxanthin, ChlB = chlorophyll b, ChlA = chlorophyll a, ABC = $\alpha\beta$-carotene (α-carotene + β-carotene), ZeaL = zeaxanthin + lutein, PON = particulate organic nitrogen, N + N = nitrate + nitrite, PO_4 = phosphate, PAR = daily mean photosynthetically active radiation experienced by cells, and T = temperature.

3.2. Reconstruction of Phytoplankton Carbon Data

The multiple regression model (equation (2)) has a modeling efficiency (ME) of 0.72–0.90 with respect to the fitted depth-resolved (PC, ProC, SynC, and EukC) data (Table 1). These can be considered "general R^2" values, evaluated on the untransformed scale (ME = 1 − SSR/SSD with SSR the sum-of-squared residuals and SSD/(n − 1) the sample variance [*Stow et al.*, 2009]; adjusting for degrees of freedom reduces ME by ~0.01). ME remains high when considering euphotic averages (Table 1). However, a stronger and more relevant test for our purposes is to compare predicted euphotic averages with data from single profiles withheld from the fit. Aggregating results over all ~30 such cross-validation tests gives MEs of 0.48–0.68 and root-mean-square errors 17–50% of sample mean values (Table 1).

Significant predictors from a bootstrap test reflect known pigment associations in some cases, e.g., zeaxanthin and chl *b* are signature pigments for *Prochlorococcus* and thus have strong positive effects on ProCr (where the "r" denotes "reconstructed"); chl *b* is absent in *Synechococcus* and thus has a negative effect on SynCr; chl $c_1 + c_2$ and 19′-butanoyloxyfucoxanthin are mostly found in eukaryote cells and thus have strong positive effects on EukCr [*Veldhuis and Kraay*, 2004; *Higgins et al.*, 2011]. Other significant predictors are, however, less intuitive and likely reflect correlations among predictor variables and the underlying species abundances.

The model closely reproduces vertical profiles of temporal means and standard deviations (Figure 2), including the vertical niche separation between the more shade-adapted *Prochlorococcus* and the more surface-dwelling *Synechococcus*/eukaryote species. A similar niche separation over seasons, with ProC blooming in Fall and SynC/EukC blooming in Winter, is also reproduced (Figure 3). Time series for each depth level show a good fit

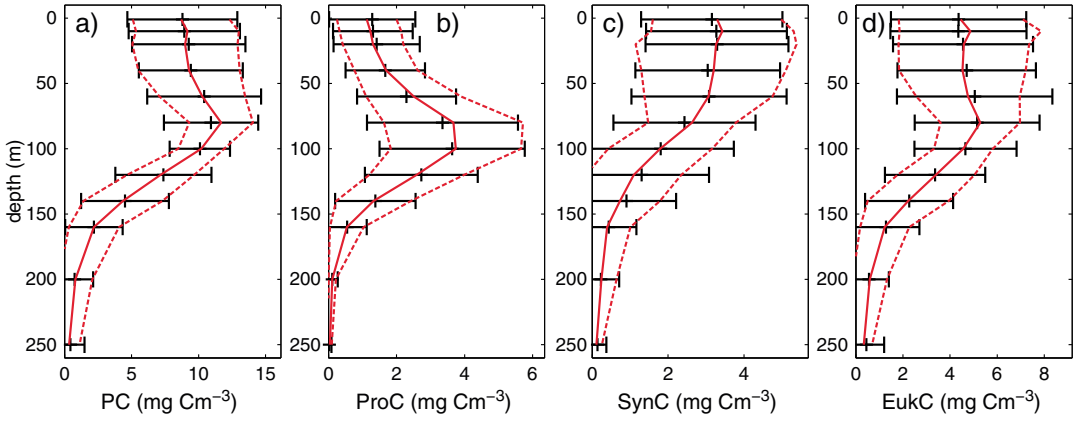

Figure 2. Profiles of temporal means ±1 standard deviation for the original seasonal-average phytoplankton carbon data (black error bars) and the corresponding reconstructed data (red envelopes). (a) PC = total phytoplankton carbon, (b) ProC = *Prochlorococcus* carbon, (c) SynC = *Synechococcus* carbon, and (d) EukC = eukaryotic phytoplankton carbon.

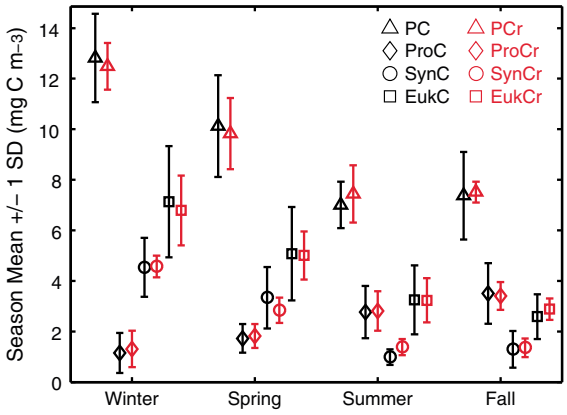

Figure 3. Single-season means ±1 standard deviation over 7-8 sampled years for the original phytoplankton carbon data, averaged over seasons and 0-140 m (black error bars), and the corresponding reconstructed data (red error bars). PC = total phytoplankton carbon, ProC = *Prochlorococcus* carbon, SynC = *Synechococcus* carbon, and EukC = eukaryotic phytoplankton carbon.

within each layer and a plausible variability beyond the data (Figure 4 shows EukCr as an example; see Figures S6–S8 for other groups and tables in the supporting information for numerical values with uncertainties). The skill statistics in Table 1, the data fit in Figures 2–4, the bootstrap prediction SEs in Figure 4, and the low levels of extrapolation implied by the hat matrix criterion all support the reconstruction model as a robust and low-bias interpolator. The model predictions prior to 2004 are also found to be broadly consistent with earlier flow-cytometry data [*DuRand et al.*, 2001], allowing for potential biases due to inconsistencies in the measurement methods (see Text S7).

3.3. Analysis of the Reconstructed Phytoplankton Carbon Time Series

Fitting equation (1) with trend and seasonal effects to the reconstructed euphotic averages reveals a significant increasing trend in PCr and weakly significant increases in ProCr and EukCr (Figure 5). Three year means show significant multiannual variability, with ProCr and SynCr decreasing in the late 1990s and increasing from the mid-2000s, while EukCr does the opposite. To measure changes in community structure, we analyze the time series of euphotic-average group carbon as a % of euphotic-average total

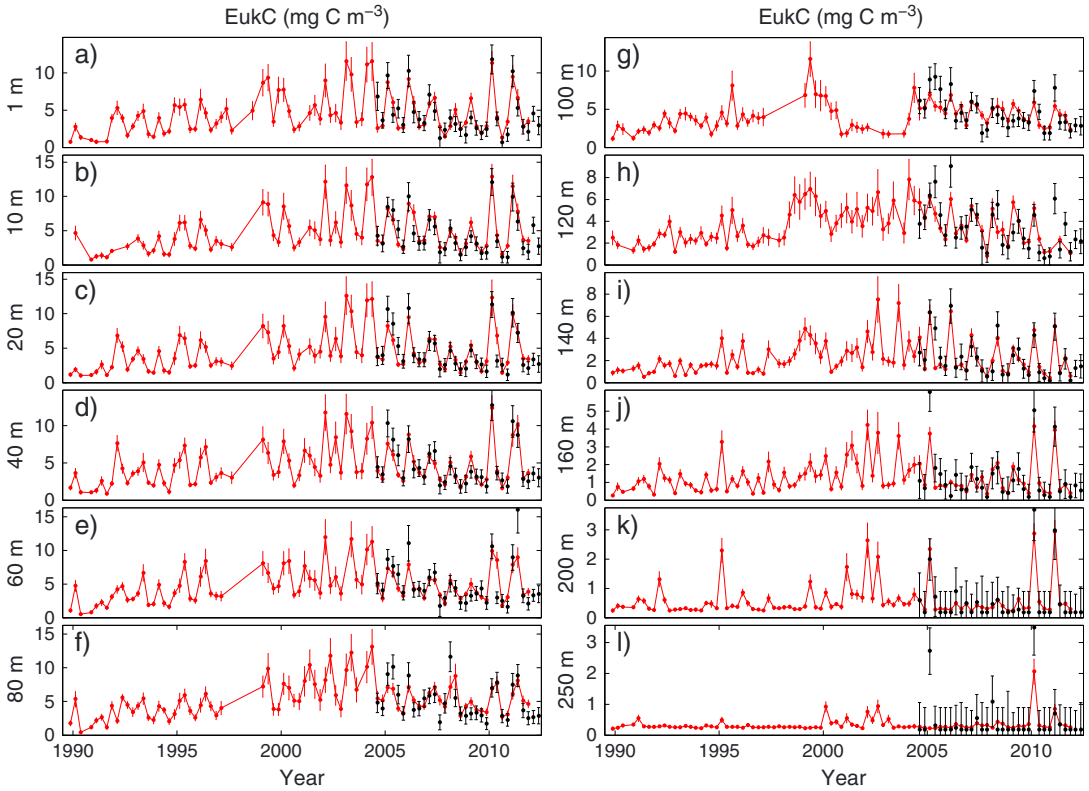

Figure 4. Time series of eukaryotic phytoplankton carbon concentrations (units mg C m^{-3}) for each of the 12 grid depths, showing the original seasonal-average data (black dots) and the reconstructed data (red dots and lines). Error bars are ±1 standard error, derived from the subseasonal sampling variance for the original data (section 2.1) and by a bootstrap method for the reconstructed data (Text S5). Predictions beyond the sampled seasons are still interpolations in the space of predictors according to the hat matrix criterion; the 5% of points classed as extrapolations are excluded, leaving gaps in the shallow and middepth series during 1997–1998.

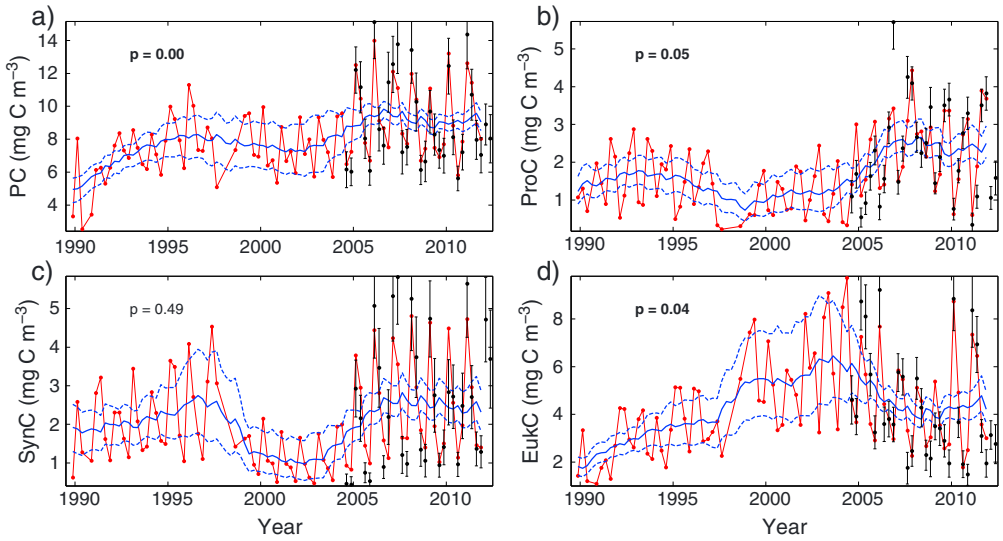

Figure 5. Time series of phytoplankton carbon concentrations averaged over seasons and 0–140 m, showing the original data (black dots, error bars are 1 SE), the reconstructed data (red dots and lines), and the 3 year means of the reconstructed data (blue lines, envelopes are 95% CIs). (a) PC = total phytoplankton carbon, (b) ProC = *Prochlorococcus* carbon, (c) SynC = *Synechococcus* carbon, and (d) EukC = eukaryotic phytoplankton carbon. *P* values are for the long-term trends in the reconstructed data (bold < 0.05). SEs in the original data are derived from the subseasonal sampling variance of the vertical averages (section 2.2); CIs in the reconstructed 3 year means are derived by a bootstrap method (Text S5).

phytoplankton carbon (to guarantee estimates < 100%, we sum over group models rather than using the PCr model). These group fractions show no significant long-term trends (Figure 6), but their 3 year means show strong multiannual variability, with the eukaryote fraction varying between ~70% during a eukaryote-dominated "phase" (1998–2005) and ~45% during prokaryote-dominated phases (1990–1997, 2006–2012, Figure 6c). These results are robust to whether or not model selection is applied and to whether or not extrapolation points are excluded (Figures S11 and S12). Moreover, the reconstruction reproduces a significant ($p = 0.04$) decreasing trend in the original EukC : PC data since 2004 (see Figure 6c).

3.4. Explaining the Long-Term Variability in Phytoplankton Biomass

We seek to explain group biomass variability on three timescales: interannual/residual variability (mainly year to year), multiannual shifts (see Figure 6c), and long-term (22 year) trends. Interannual variability in Sargasso Sea phytoplankton abundance is often explained by variations in nutrient supply [*Bates*, 2001; *Oschlies*, 2001; *Follows and Dutkiewicz*, 2002; *Lomas and Bates*, 2004; *Krause et al*., 2009; *Lomas et al*., 2010a, 2013; *Lozier et al*., 2011; *Patara et al*., 2011]. We argue, however, that nutrient supply alone may not suffice to explain the variability in community structure. Indeed, on the seasonal scale (see Figure 3), the winter blooms of *Synechococcus* and eukaryote species may be explained by nitrate supply from convective mixing, but the winter minima in *Prochlorococcus* abundance are probably best explained by mixing-induced light shock [*DuRand et al*., 2001; *Malmstrom et al*., 2010; *Casey et al*., 2013], although temperature changes, grazing, viral lysis, and copper toxicity may also play a role [*DuRand et al*., 2001; *Mann et al*., 2002; *Parsons et al*., 2012; *Casey et al*., 2013]. Compared to *Synchecococcus*, the photophysiology of *Prochlorococcus* has less resistance to photoinactivation and oxidative stress [*Mella-flores et al*., 2012] and slower rates of repair after photoinhibition [*Six et al*., 2007; *Mella-flores et al*., 2012], resulting in greater vulnerability to light shock, especially in low-light adapted ecotypes [*Six et al*., 2007; *Malmstrom et al*., 2010].

3.4.1. Interannual/Residual Variability

Consider first the residuals correlations of explanatory variables with chl *a* and PP, for which long ($n \sim 90$) series of original data are available (Table 2). Recall that seasonal, multiannual shift, and trend effects have all been removed by fitting the time series model. The strongest correlations over all seasons are with mesozooplankton abundance (Z) ($r = 0.3$–0.4, $p < 0.05$) and suggest bottom-up control via food supply rather than top-down control via grazing pressure. This is consistent with gut content analyses which show that phytoplankton can be a significant food source even for the larger (>2 mm) mesozooplankton, at least during winter/spring

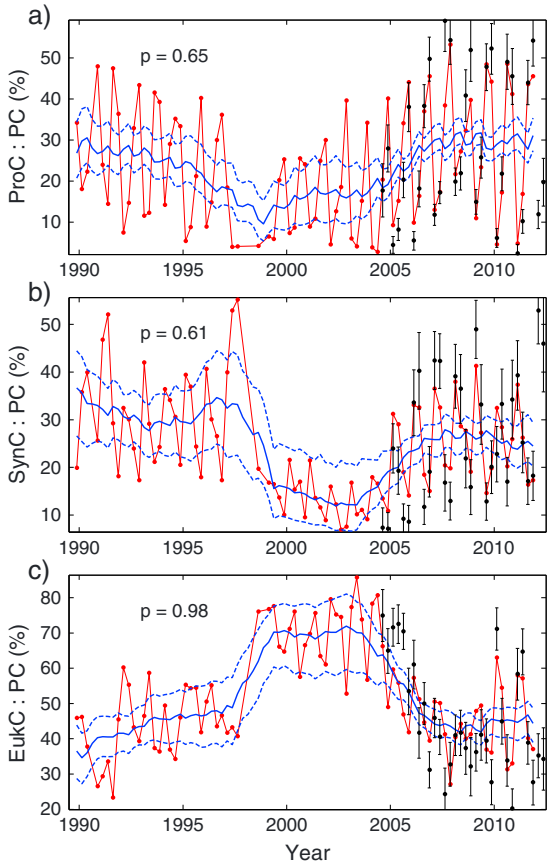

Figure 6. Time series of phytoplankton carbon group fractions (ratios of seasonal and 0–140 m averages), showing the original data (black dots, error bars are 1 SE), the reconstructed data (red dots and lines), and the 3 year means of the reconstructed data (blue lines, envelopes are 95% CIs). (a) ProC:PC = *Prochlorococcus* carbon fraction, (b) SynC:PC = *Synechococcus* carbon fraction, and (c) EukC:PC = eukaryotic phytoplankton carbon fraction. *P* values are for the long-term trends in the reconstructed data (bold < 0.05). SEs in the original data are derived from the subseasonal sampling variance (section 2.2) and application of the delta method, assuming independent errors between groups. CIs in the reconstructed 3 year means are derived by a bootstrap method (Text S5).

[*Schnetzer and Steinberg*, 2002]. It also agrees with observations that mesozooplankton grazing control is highly seasonal and never strong: *Roman et al.* [1993] measured grazing by >200 μm zooplankton on >2 μm phytoplankton as 2 and 57 mg C m^{-2} d^{-1} in August and March/April, amounting to 1% and 17% of total primary production during those months [*Malone et al.*, 1993]. Strong negative correlations are also observed with heat content (T) and stratification index ($\Delta\rho$) in winter ($r \sim -0.4$ to -0.7, $p < 0.05$). The fact that both chl *a* and PP show these correlations suggests a growth response to nutrients supplied by deeper (and cooler and denser) waters, rather than only mixing-induced photoadaptation. Correlations with N + N and PO_4 are positive but generally weaker, possibly due to undersampling and/or the decoupling of nutrient uptake from carbon assimilation, allowing PP to remain high after rapid consumption of vertically imported nutrients [*Mongin et al.*, 2003]. There are, however, moderate springtime correlations between PP and N + N ($r = 0.47$, $p < 0.05$) and POCN ($r = -0.43$, $p = 0.05$), suggesting nitrogen limitation. There is also a strong correlation between chl *a* and PO_4 in fall ($r = 0.53$, $p < 0.01$), perhaps reflecting a growth response of deeper-dwelling phytoplankton with high chl *a*: carbon ratios and minor contributions to PP (r is insignificant for the 0–70 m layer). Despite the implied nutrient supply, MLD does not significantly correlate with PP for any or all seasons, possibly due to undersampled MLD fluctuations [*Lomas et al.*, 2009] and/or photodamage of cells mixed toward the surface then trapped in the C14 incubation bottles. There are, however, positive correlations between $MLD_{1,2}$ and chl *a*, especially in summer ($r = 0.48$, $p < 0.05$), likely reflecting photoadaptation to reduced average light levels. Significant winter correlations between the NAO index and chl *a* ($r = -0.45$) and PP ($r = -0.58$) are consistent with increased nutrient supply during low-NAO winters [*Bates*, 2001].

Correlation analyses with the original carbon data (PC, etc.) are severely limited by sample size ($n \sim 30$ or 7–8 within seasons). Nevertheless, highly significant ($p < 0.01$) correlations are observed between ProC and (T, $\Delta\rho$) ($r \sim 0.5$), especially in winter ($r \sim 0.9$) when a strong negative correlation with MLD_2 is also observed ($r \sim -0.9$). These are consistent with the mixing-induced light shock mechanism proposed above to explain the seasonal minima. We also observe significant ($p < 0.05$) negative correlations between EukC and T ($r = -0.38$), especially in winter ($r = -0.81$), and a positive correlation with PO_4 over all seasons ($r = 0.37$), consistent with growth responses to increased nutrient supply by vertical exchange. Although the only significant correlation with mesozooplankton (Z) is for SynC in fall ($r = 0.83$, $p < 0.05$), there are marginal winter correlations with EukC ($r = 0.76$, $p = 0.08$) and with ProC ($r = -0.80$, $p = 0.05$), consistent with bottom-up control via food supply from the larger algae which flourish in conditions unfavorable to *Prochlorococcus*.

Residual correlations with the reconstructed data (not shown) are of questionable significance because some of the explanatory variables were used as predictor variables in the reconstruction. They are nevertheless

Table 2. Significant Interannnual/Residual Correlations Between Phytoplankton Biomass and Explanatory Variables[a]

Variable	All Seasons	Winter	Spring	Summer	Fall
ChlA	**$Z^{(+)}$**, $T^{(-)}$, $PO_4^{(+)}$, $MLD_2^{(+)}$	**$T^{(-)}$**, $NAO^{(-)}$, $\Delta\rho^{(-)}$	–	$MLD_1^{(+)}$	**$PO_4^{(+)}$**, $Z^{(+)}$
PP	**$T^{(-)}$**, $Z^{(+)}$, $N+N^{(+)}$, $WS^{(+)}$, $NAO^{(-)}$	**$\Delta\rho^{(-)}$**, **$T^{(-)}$**, **$NAO^{(-)}$**	$N+N^{(+)}$	–	–
PC	–	–	–	–	–
ProC	**$T^{(+)}$**, **$\Delta\rho^{(+)}$**	**$T^{(+)}$**, **$MLD_2^{(-)}$**, **$\Delta\rho^{(+)}$**	$NAO^{(-)}$	–	–
SynC	–	–	–	$\Delta\rho^{(-)}$	$Z^{(+)}$
EukC	$T^{(-)}$, $PO_4^{(+)}$	$T^{(-)}$	–	–	$NAO^{(+)}$
$ChlA_{Pro}$	$Z^{(+)}$, **$T^{(-)}$**, $PO_4^{(+)}$	–	$PO_4^{(+)}$, $T^{(-)}$	$MLD_1^{(+)}$	$PO_4^{(+)}$
PP_{Pro}	**$T^{(-)}$**, **$Z^{(+)}$**, **$N+N^{(+)}$**, $WS^{(+)}$, $POCN^{(-)}$, $\Delta\rho^{(-)}$	$\Delta\rho^{(-)}$, **$NAO^{(-)}$**, **$T^{(-)}$**, $PO_4^{(+)}$, $WS^{(+)}$	**$T^{(-)}$**, $Z^{(+)}$, $N+N^{(+)}$, $POCN^{(-)}$	**$N+N^{(+)}$**	–
$ChlA_{Euk}$	–	–	$MLD_1^{(+)}$	$Z^{(+)}$	$\Delta\rho^{(+)}$
PP_{Euk}	–	–	–	$PO_4^{(-)}$	–

[a]Significant zero-lag Pearson correlations are shown ($p < 0.05$, bold where $p < 0.01$) between subsetted prewhitened residuals from time series model fits to data from all seasons, including seasonal, multiannual shift, and trend effects. Correlations are ordered by decreasing magnitude, with signs indicated by superscripts. Biomass variables include chlorophyll *a* (ChlA), primary productivity (PP), total phytoplankton, *Prochlorococcus*, *Synechococcus*, and eukaryote carbon (PC, ProC, SynC, and EukC) and the (ChlA and PP) restricted to the prokaryote/eukaryote phases ($ChlA_{Pro/Euk}$ and $PP_{Pro/Euk}$). Explanatory variables include nitrate-plus-nitrite (N + N), phosphate (PO_4), particulate organic carbon : nitrogen (POCN), water temperature (*T*), surface wind speed at Bermuda Airport (WS), mixed layer depth via a 0.2°C or 0.02°C variable sigma-*t* criterion (MLD_1 and MLD_2), density stratification between 0 and 200 m ($\Delta\rho$), the North Atlantic Oscillation index (NAO), and the total mesozooplankton biomass (Z). Variables are averages over seasons and where applicable the surface 0–140 m layer (Z is an average over a tow depth of 150–200 m [*Steinberg et al.*, 2012]).

coherent with the original data analysis: EukCr is stimulated, and ProCr suppressed, in years with strong vertical exchange (especially during winter/spring), and correlations with Z are consistent with bottom-up control by the larger phytoplankton. We also considered correlations restricted to the prokaryote phases (prior to 1997 and after 2006) and to the eukaryote phase (between 1998 and 2005) for the variables (ChlA, PP) with sufficient data coverage. Compared to the unrestricted analysis, additional significant spring/summer correlations are observed, despite the reduced sample size, between $ChlA_{Pro}$ and (PO_4, *T*) and between PP_{Pro} and (*T*, Z, N + N, POCN), suggesting a stronger coupling to spring/summer nutrient supply during the prokaryote phases (Table 2). Correlations during the eukaryote phase are limited by sampled size, but the springtime correlation of $ChlA_{Euk}$ with MLD_1 may reflect mixing-induced photoadaptation (see below).

Table 3. Multiannual Shifts in Phytoplankton Biomass and Explanatory Variables[a]

	All Seasons	Winter	Spring	Summer	Fall
			Biomass Variables		
ChlA	10 (−9 to 32)	10 (−22 to 42)	−5 (−32 to 28)	**17 (−2 to 37)**	15 (−20 to 57)
PP	9 (−8 to 28)	−2 (−37 to 52)	−3 (−29 to 28)	18 (−29 to 54)^{LB}	*25 (−9 to 62)*
PCr	−6 (−19 to 9)	−11 (−30 to 7)	−9 (−35 to 26)	0 (−17 to 15)	**−17 (−27 to −4)***
ProCr	**−48 (−62 to −31)***	*−40 (−68 to 19)*	**−59 (−74 to −39)***	**−55 (−78 to −22)***	**−34 (−52 to −11)***^{L}
SynCr	**−45 (−59 to −21)***	**−54 (−65 to −39)***	*−42 (−69 to 14)*	*−39 (−62 to 8)*	**−58 (−67 to −38)***
EukCr	**67 (34 to 110)***	**43 (18 to 74)***	**75 (21 to 170)***	**92 (44 to 153)***	**47 (22 to 85)***
			Explanatory Variables		
N + N	−19 (−41 to 8)	21 (−52 to 126)	10 (−39 to 77)	**−54 (−67 to −34)***^{L}	−24 (−53 to 22)
PO_4	−14 (−37 to 19)	7 (−30 to 64)^{L}	−4 (−38 to 49)	**−41 (−51 to −6)***	−17 (−47 to 43)
POCN	**24 (7 to 46)***	16 (−9 to 40)	**29 (3 to 55)**	*15 (−4 to 46)*	*28 (−6 to 66)*^{KB}
T (°C)	**0.3 (0.0 to 0.6)**^{KB}	0.4 (−0.2 to 1.2)	0.2 (−0.2 to 0.7)	**0.5 (0.1 to 0.9)**	0.1 (−0.4 to 0.6)
WS	2 (−2 to 7)	6 (−3 to 21)	−3 (−12 to 6)	3 (−3 to 9)	4 (−7 to 14)
MLD_1	11 (−33 to 58)	*−25 (−47 to 8)*^{LB}	**41 (8 to 79)***	14 (−9 to 37)	−9 (−25 to 8)
MLD_2	17 (−29 to 62)	*−34 (−60 to 10)*	**64 (5 to 152)**	19 (−15 to 64)^{LB}	*−9 (−18 to 1)*
$\Delta\rho$	−2 (−6 to 2)	3 (−11 to 18)	**−8 (−14 to −2)***	−1 (−5 to 3)	−1 (−7 to 5)^{LB}
NAO	−0.1 (−1.1 to 0.8)	−0.6 (−2.4 to 0.9)^{LB}	0.7 (−0.8 to 2.3)	*−0.9 (−2.0 to 0.3)*	0.3 (−2.2 to 2.9)
Z	**28 (10 to 53)***	*49 (−3 to 120)*	28 (−12 to 94)	*34 (−6 to 80)*^{LB}	3 (−23 to 34)

[a]All shifts are % changes except for *T* (units °C) and NAO (dimensionless) (see Table 2 for variable abbreviations). Ranges show 95% CIs, and font indicates the shift significance (italics where $0.05 < p < 0.15$, bold where $p < 0.05$, bold with asterisk where $p < 0.01$). Superscripts denote failed tests of time series model adequacy ($p < 0.05$): L = Lilliefors test of normality, KB = Koenker-Bassett test for homogeneity of variance, and LB = Ljung-Box test for adequacy of the AR1 correlation model.

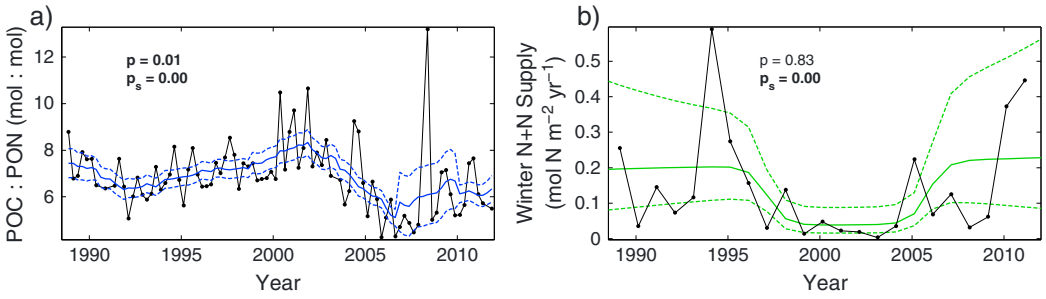

Figure 7. Time series of the molar ratio of (a) particulate organic carbon to particulate organic nitrogen, averaged over seasons and the euphotic layer 0–140 m, and (b) the estimated wintertime supply of nitrate-plus-nitrite (N + N) to the euphotic layer by convective entrainment. *P* values are for the long-term trends (*p*) and multiannual shifts (p_s) (bold < 0.05). Figure 7a shows the seasonal data (black dots) and their 3 year running means (blue lines, envelopes are 95% CIs derived from the subseasonal sampling variance). Figure 7b shows estimates of winter N + N supply using the product of the maximum winter mixed layer depth (as a monthly average) and the previous fall N + N averaged over the same depth (black dots, no error estimates) as well as the mean variability from the fitted time series model (green lines, envelopes are 95% CIs).

3.4.2. Multiannual Shifts

Multiannual shifts in chl *a*, primary productivity (PP), and reconstructed total carbon (PCr) are generally weak and insignificant (Table 3). By contrast, strong multiannual shifts are observed in all reconstructed group biomasses in all seasons individually and together. The reconstructed shift in community structure (Figure 6) therefore results from significant decreases in both ProCr and SynCr as well as a significant increase in EukCr (Figures 5b–5d).

One hypothesis to explain this shift is an overall increase in nutrient supply during the eukaryote phase (1998–2005). There is, however, little evidence in the explanatory variables to support this hypothesis (Table 3). During the eukaryote phase, dissolved inorganic nutrients (N + N, PO_4) show an overall (nonsignificant) decrease, with the decrease most pronounced in summer. As discussed above, nutrient concentrations may drop with an increase in nutrient supply due to the stimulation of biological uptake. However, the observed positive residual correlations between (chl *a*, EukC) and (N + N, PO_4) (see above) suggest that, for the seasonal averages considered here, the growth response is not strong enough to reverse the positive correlation between (N + N, PO_4) and nutrient supply. Moreover, the significant increase in particulate organic carbon : nitrogen (POCN) suggests an increase in community nitrogen stress, hence a reduction in nutrient supply, during the eukaryote phase (Table 3 and Figure 7a), and no significant increases are observed in PP (Table 3) or the bulk growth rate μ = PP/PCr (not shown). Furthermore, an overall increase in nutrient supply is not supported by the physical variables. Winter mixed layer depths were significantly shallower during the eukaryote phase (Figures 8a and 8d), suggesting a reduction in annual nutrient supply by convective entrainment, which was the dominant supply mechanism in eddy-resolving simulations [*Oschlies*, 2002; *McGillicuddy et al*., 2003]. A simple estimate of winter N + N supply using the product of the maximum winter MLD_1 (as a monthly average, similar results using raw values) and the previous fall N + N averaged over the same depth supports a roughly threefold reduction during the eukaryote phase (Figure 7b; cf. *Siegel et al*. [1999] mean estimate of 0.17 mol N m^{-2} yr^{-1} for the years 1989–1995). Heat content (*T*) was also higher during the eukaryote phase (Table 3 and Figures S5t and S5u in the supporting information), shifts in wind speed (WS), stratification index ($\Delta\rho$) and NAO index were insignificant (Table 3), and surface geostrophic + Ekman velocity estimates [*Bonjean and Lagerloef*, 2002, not shown] did not support a shift in contributions from horizontal advection (though this neglects changes in lateral gradients). Finally, even if nutrient supply were increased (e.g., by vertical migration, see *Fawcett et al*. [2014]), this alone would not explain the reduced prokaryote biomass (Figures 5b and 5c), nor perhaps the factor of 2 lower carbon per cell (Figures 1g and 1h). Laboratory experiments on cultured strains have found that prokaryote carbon per cell may increase with phosphorus stress, perhaps due to an inability of undernourished cells to replicate chromosomes and divide [*Bertilsson et al*., 2003]; however, flow-cytometry data for field samples from the Sargasso Sea have shown small increases in prokaryote forward light scatter (hence cellular carbon) with nutrient amendment [*Worden and Binder*, 2003].

We suggest that the shift in community structure may have been largely driven by a shift in the seasonality of mixing. Mixed layer depths show no significant all-season shifts, but there are strong decreases in winter

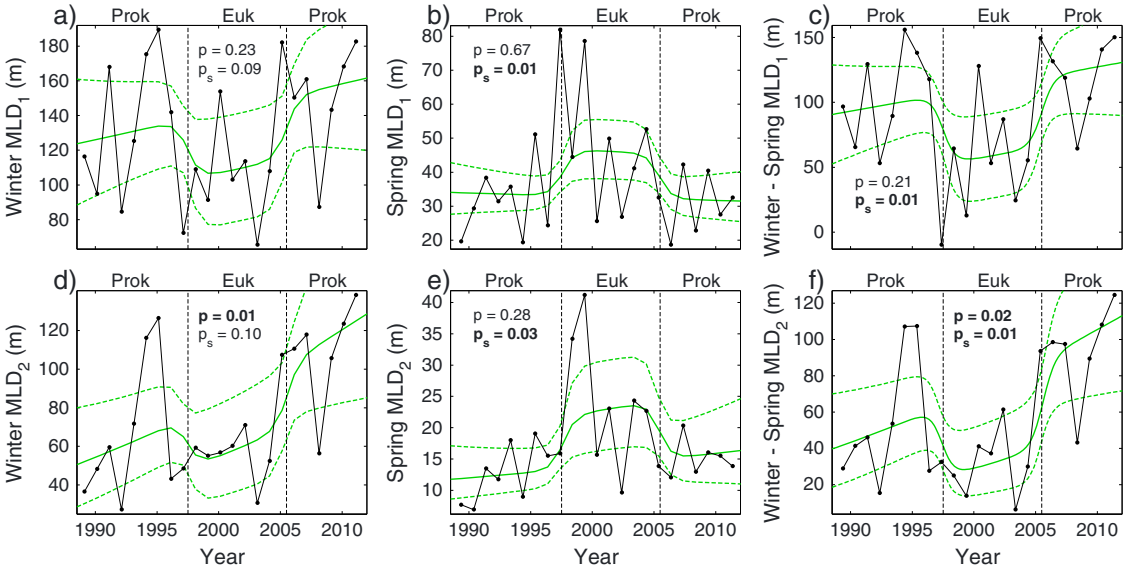

Figure 8. Single-season time series of mixed layer depths from variable sigma-*t* criteria equivalent to ΔT = (a–c) 0.2°C or (d–f) 0.02°C for winter (Figures 8a and 8d), spring (Figures 8b and 8e), and the difference (Figures 8c and 8f). Black dots show seasonal means, and green lines show mean variability from the fitted time series model (envelopes are 95% CIs). *P* values are for the long-term trends (*p*) and multiannual shifts (p_s) (bold < 0.05). Vertical dotted lines show transition times between prokaryote (Prok) and eukaryote (Euk) phases.

$MLD_{1,2}$ and increases in spring $MLD_{1,2}$ (Table 3 and Figure 8), resulting in significantly reduced winter-spring shoaling (Figures 8c and 8f). The weak significance of some of these shifts may reflect data noise due to the undersampling of high-frequency variability [*Lomas et al*., 2009] (SEs in seasonal means are mostly 20–30 m). Increased mixing in spring, when surface irradiances are ~60% higher than in winter, may have exacerbated light shock to unsustainable levels for *Prochlorococcus*, causing the crash in ProC during 1997 (Figures 5b and 8b) and suppressing biomass in subsequent years, possibly with interannual effects on seed populations. This would also explain the reduction in *Prochlorococcus* carbon per cell (Figure 1g), since the larger, low-light adapted ecotypes are more prone to light shock mortality. It is curious that we observe similar depressions of *Synechococcus* biomass (Figure 5c) and carbon per cell (Figure 1h), as these prokaryotes should be substantially more resistant to light shock (see above). Many eukaryotes (algae), however, can thrive in fluctuating light environments, thanks to efficient xanthophyll cycle photoprotection mechanisms, thought to be more powerful than those of cyanobacteria [*Brunet and Lavaud*, 2010; *Kulk et al*., 2011]. Such algae may in fact have benefited from higher average light levels in winter (due to reduced mixing), a more even seasonal pattern of nutrient supply (albeit less in total), increased irradiance during nutrient supply events, and less sustained surface exposure in spring. Possible evidence of a light shock response in the eukaryote community is provided by the time series for the pigments diadinoxanthin and diatoxanthin which are associated with xanthophyll cycles in some algal cells (Figures S5h and S5i). Diadinoxanthin shows a highly significant increase in 3 year mean values around the onset of the eukaryote phase, although the anomaly relaxes by winter 1999 (Figure S5h). Diatoxanthin shows a highly significant positive multiannual shift ($p < 0.001$, Figure S5i), although the shift is not significant when considering the ratio to EukCr and may thus only reflect the overall increase in eukaryotic biomass. Also, the shift in mixing seasonality may not have favored eukaryotes with permanently higher xanthophyll cycle pigment content but rather those with the capacity to vary their cellular content of these pigments in response to springtime mixing through strong vertical light gradients [*Polimene et al*., 2013].

Regarding top-down control, there is no direct evidence that the increase in EukC resulted from reduced grazing pressure; rather, mesozooplankton biomass (Z) appears to have increased during the eukaryote phase (Table 3). It is however possible that enhanced carnivory by mesozooplankton reduced the grazing pressure from <200 μm microzooplankton/nanozooplankton, which were likely the dominant grazers, at least during summer [*Roman et al*., 1993; *Lessard and Murrell*, 1998] (note also that the largest relative increase in EukC occurred in summer, Table 3). On the other hand, the hypothesis of top-down control would then demand a top-down explanation for the increased Z (see discussion in *Steinberg et al*. [2012]). Grazing on algae may also have reduced due to lower food quality driven by reduced nutrient supply (see above),

Table 4. Trend Increases in Phytoplankton Biomass and Explanatory Variables[a]

	All Seasons	Winter	Spring	Summer	Fall
			Biomass Variables		
ChlA	**56 (21 to 111)***	**69 (10 to 127)***	**58 (7 to 166)**	10 (−16 to 47)	*69 (−10 to 201)*
PP	15 (−10 to 41)	45 (−27 to 188)	12 (−23 to 67)	14 (−40 to 81)^{LB}	−6 (−37 to 36)
PCr	**53 (28 to 89)***	**66 (20 to 121)***	**63 (5 to 187)**	*21 (−3 to 57)*	**30 (16 to 57)***
ProCr	**83 (38 to 155)***	0 (−67 to 131)	**113 (36 to 231)***	**70 (−16 to 255)**	**91 (39 to 185)*^{L}**
SynCr	30 (−16 to 93)	**72 (36 to 130)***	34 (−44 to 222)	−21 (−61 to 94)	**50 (10 to 111)***
EukCr	**73 (29 to 135)***	**128 (57 to 229)***	**105 (3 to 415)**	37 (−17 to 129)	26 (−16 to 86)
			Explanatory Variables		
N + N	23 (−17 to 81)	−26 (−76 to 158)	−30 (−64 to 44)	**112 (31 to 236)*^{L}**	*80 (−6 to 213)*
PO_4	22 (−20 to 81)	−3 (−45 to 64)^{L}	37 (−27 to 134)	−14 (−36 to 22)	30 (−35 to 142)
POCN	**−20 (−33 to −7)***	−11 (−33 to 19)	−7 (−25 to 21)	**−28 (−47 to 11)**	*−27 (−54 to 15)*^{KB}
T (°C)	0.1 (−0.3 to 0.4)^{KB}	*−0.6 (−1.7 to 0.2)*	−0.1 (−0.8 to 0.4)	−0.1 (−0.6 to 0.4)	**0.9 (0.2 to 1.5)***
WS	**10 (4 to 15)***	*9 (−6 to 23)*	*9 (−4 to 21)*	**12 (4 to 20)***	*9 (−5 to 22)*
MLD_1	3 (−56 to 57)	25 (−15 to 75)^{LB}	−6 (−30 to 27)	−6 (−28 to 27)	3 (−17 to 27)
MLD_2	**85 (27 to 144)***	**120 (15 to 300)**	33 (−26 to 140)	23 (−30 to 98)^{LB}	**21 (6 to 38)***
$\Delta\rho$	1 (−4 to 7)	*−13 (−27 to 4)*	−1 (−10 to 8)	3 (−2 to 8)	**9 (2 to 16)**^{LB}
NAO	−0.7 (−1.8 to 0.5)	**−2.1 (−4.0 to 0.1)**^{LB}	−0.5 (−2.5 to 1.8)	−0.3 (−1.8 to 1.1)	0.4 (−2.9 to 4.4)
Z	**117 (64 to 192)***	**170 (50 to 573)***	**115 (5 to 535)**	*89 (−13 to 384)*^{LB}	**57 (−3 to 163)**

[a] All trend increases are % changes except for T (units °C) and NAO (dimensionless) (see Table 2 for variable abbreviations). Ranges show 95% CIs, and font indicates the shift significance (italics where $0.05 < p < 0.15$, bold where $p < 0.05$, bold with asterisk where $p < 0.01$). Superscripts denote failed tests of time series model adequacy ($p < 0.05$): L = Lilliefors test of normality, KB = Koenker-Bassett test for homogeneity of variance, and LB = Ljung-Box test for adequacy of the AR1 correlation model.

though again this would not explain the increased Z. Grazing on ProC/SynC may have increased due to reduced algal food quality or increased microzooplankton/nanozooplankton, possibly fueled by the increased EukC. Grazing on Sargasso Sea prokaryotes has been observed to increase with food quality [*Worden and Binder*, 2003], but this would not appear consistent with the observed decreases in carbon per cell (Figures 1g and 1h) and the apparent reduction of nutrient supply (see above). Alternatively, the increased algal biomass and reduced nutrient supply may have increased grazing pressure from mixotrophs: algal bacterivory is widely observed in the Atlantic Ocean [*Hartmann et al.*, 2012], algal grazing of picocyanobacteria has been observed in the Sargasso Sea [*Arenovski*, 1994; *Sanders et al.*, 2000], and [*Frias-Lopez et al.*, 2009] identified prymnesiophytes —likely the dominant algae at BATS—as major grazers of picocyanobacteria in the surface waters of the Pacific Ocean. However, if mixotrophy were the main cause of the negative prokaryote shifts, we would expect these shifts to be more pronounced in the nutrient-depleted surface waters [*Arenovski*, 1994]. In fact, analysis of the time series at individual depths reveals an increasing trend with depth to 140 m in the magnitude of the estimated prokaryote shift (linear regression, $p = 0.06/0.07$ for ProC/SynC), which is more consistent with the mixing-induced light shock hypothesis. On the other hand, an increase in eukaryote mixotrophy might better explain the weakened coupling between (ChlA and PP) and nutrient supply proxies (Table 2), and perhaps also the strong negative shift in SynCr (Figure 5c).

3.4.3. Long-Term Trends

Highly significant increasing trends are observed in chl *a* and most carbon groups (Figures 5 and S5l and Table 4), but biomass fractions show no significant trends (Figure 6; these results are insensitive to whether or not a shift effect is fitted). Primary productivity has, however, only weakly increased, suggesting a decrease in the bulk phytoplankton growth rate, which is confirmed by the time series for $\mu = PP/PCr$ ($T = -31\%$, $p = 0.01$). This may reflect a change in eukaryote community structure, since there is little evidence of decreasing nutrient supply (Table 4) or surface irradiance (not shown), and biogenic silica—a proxy for diatom abundance [*Krause et al.*, 2009]—shows a strongly decreasing trend ($T = -62\%$, $p = 0.006$).

To explain the increasing biomass trends, nutrients and heat content show no significant all-season trends nor is there evidence of an increase in the peak mixing events which set the mixed layer depth MLD_1 (Table 4) or the annual convective nitrogen supply (Figure 7b). However, we do observe a significant decreasing trend in POCN (Figure 7a), suggesting a gradual relief of nitrogen stress. We also observe significant increasing trends in surface wind speed (WS) [cf. *Bates*, 2007] and winter mixing layer depth MLD_2 (Figure 8d), supporting a gradual increase in nutrient supply from moderate, wind-driven convective and diffusive events [*Lomas et al.*, 2010a, 2013]. The increase in the rate of supply during such events may have been small compared to uptake losses except when

primary productivity was lower in summer/fall, hence the increasing N + N trends only in these seasons (Table 4). Over the period 1990–2012, a significant decreasing trend is also observed in the winter NAO index (Table 4), consistent with an increasing frequency (but not necessarily intensity) of storms arriving at the BATS site. Despite the increases in fall wind speed and mixing layer depth, fall heat content (T) appears to have increased by around 0.5°C per decade, implying an increase in fall stratification ($\Delta\rho$ also shows a weak positive trend) which might explain the stronger increase in ProC than in SynC. Mesozooplankton abundance (Z) has also strongly increased, suggesting bottom-up control on Z, although this trend may also have top-down drivers [*Steinberg et al*., 2012] and may have facilitated the phytoplankton increase via predation on smaller grazers.

4. Conclusions

We have analyzed 1990–2012 time series of phytoplankton pigments and group carbon biomass in the Sargasso Sea, using recent flow-cytometric measurements and a multiple regression approach to reconstruct carbon concentrations prior to 2004. Year-to-year biomass variations were apparently driven by the intensity of winter mixing, controlling the supply of nutrients for eukaryote blooms and the severity of *Prochlorococcus* minima, and in turn correlated with the winter NAO index. Group carbon time series also showed strong multiannual variability, with the eukaryote biomass fraction varying from ~45% to ~70% between prokaryote and eukaryote phases. Surprisingly, the eukaryote phase did not appear to result from an overall increase in nutrient supply—rather, winter convective entrainment was reduced and annual average nitrogen stress was elevated during this period. Instead, we hypothesize that a shift in the seasonal pattern of vertical mixing may have stimulated and restructured the algal community by reducing the seasonality of nutrient supply, while also suppressing prokaryote populations by exacerbating light shock and grazing mortality. Significant increasing trends of ~ +3% per year were observed in both chlorophyll *a* and total phytoplankton carbon, apparently fueled by a gradual increase in nutrient supply by moderate, wind-driven mixing events associated with a decreasing winter NAO index. There was little evidence of trends in eukaryote or prokaryote biomass fractions, but there was some evidence of long-term changes in the eukaryote community structure.

Understanding the mechanisms that produce long-term variability in plankton biomass is critical if we are to predict with any confidence the response of the ocean biosphere to climatic variations. The basic response of increased nutrient supply to the surface Sargasso Sea with negative swings in the NAO appears to be reproducible in mechanistic models [*Oschlies*, 2001; *Patara et al*., 2011; *Keller et al*., 2012], but it remains to be seen whether such models can reproduce the observed increasing trends in phytoplankton biomass at the BATS site. We stress that these 22 year trends do not contradict the evidence from observations [*Polovina et al*., 2008; *Boyce et al*., 2010] and models [*Steinacher et al*., 2010; *Hofmann et al*., 2011; *Yool et al*., 2013] for a longer-term anthropogenic decline in subtropical gyre productivity due to increasing stratification and decreasing nutrient supply. They do however underscore the need for longer time series and spatial averaging in order to separate such climate change signals from multidecadal variability. The observed multiannual shifts in community structure may, we suspect, prove a strong challenge for current models to reproduce due to uncertainties in parameterizing prokaryote photodamage and (possibly mixotrophic) grazing mortality. These processes could nevertheless be important in determining the structure of future marine planktonic ecosystems and the fate of nutrients supplied, impacting the balance between rapid recycling and the transfer of carbon to higher trophic levels or export to depth.

A likely prerequisite of such understanding is an improvement in the global-scale measurement of group phytoplankton biomass in terms of carbon concentration. Our study suggests that standard in situ measurements, including HPLC pigments, temperature, and light levels, may be used to reconstruct group-resolved phytoplankton carbon data, given adequate direct measurements (e.g., from flow cytometry) to constrain the model. Such in situ models may then facilitate global remote sensing estimates by increasing calibration and validation matchups for algorithm development or by providing second stage estimates after remote sensing of pigments and other predictor variables [*Sathyendranath et al*., 2005; *Pan et al*., 2010; *Moisan et al*., 2013].

Acknowledgments

5P.W. and V.G. would like to acknowledge financial support from Marie Curie project 252095. J.R.C. acknowledges support from the National Science Foundation Graduate Research Fellowship (DGE-1329626). M.W.L. thanks the National Science Foundation Chemical and Biological Oceanography Programs for continued support of the BATS program, particularly through the most recent award OCE 0752366. The authors thank the captains and crews of the R/Vs *Cape Henlopen*, *Cape Hatteras*, *Weatherbird I* and *II*, *Oceanus*, *Edwin Link*, and *Atlantic Explorer* as well as the BATS technicians and scientists, past and present, whose diligence and dedication have resulted in the generation of the data set presented in this manuscript. We thank Ian Currie and the Bermuda Weather Service for providing cloud coverage and surface wind speed data, and the three anonymous reviewers for their constructive criticism. The one-third degree OSCAR surface current velocity data were obtained from JPL physical laboratory DAAC and developed by ESR.

References

Abrevaya, J. (2002), Computing marginal effects in the Box–Cox Model, *Econ. Rev.*, *21*(3), 383–393, doi:10.1081/ETC.-120015789.

Arenovski, A. L. (1994), Distribution, abundance and Ecology of mixotrophic algae in marine and freshwater plankton communities, PhD thesis, MIT/WHOI, WHOI-94-22.

Bates, N. R. (2001), Interannual variability of oceanic CO_2 and biogeochemical properties in the western North Atlantic subtropical gyre, *Deep Sea Res., Part II*, *48*(8–9), 1507–1528, doi:10.1016/S0967-0645(00)00151-X.

Bates, N. R. (2007), Interannual variability of the oceanic CO_2 sink in the subtropical gyre of the North Atlantic Ocean over the last 2 decades, *J. Geophys. Res.*, *112*, C09013, doi:10.1029/2006JC003759.
Bates, N. R. (2012), Multi-decadal uptake of carbon dioxide into subtropical mode water of the North Atlantic Ocean, *Biogeosciences*, *9*(7), 2649–2659, doi:10.5194/bg-9-2649-2012.
Bates, N. R., M. H. P. Best, K. Neely, R. Garley, A. G. Dickson, and R. J. Johnson (2012), Detecting anthropogenic carbon dioxide uptake and ocean acidification in the North Atlantic Ocean, *Biogeosciences*, *9*(7), 2509–2522, doi:10.5194/bg-9-2509-2012.
Behrenfeld, M. J., E. Boss, D. A. Siegel, and D. M. Shea (2005), Carbon-based ocean productivity and phytoplankton physiology from space, *Global Biogeochem. Cycles*, *19*, GB1006, doi:10.1029/2004GB002299.
Behrenfeld, M. J., R. T. O'Malley, D. A. Siegel, C. R. McClain, J. L. Sarmiento, G. C. Feldman, A. J. Milligan, P. G. Falkowski, R. M. Letelier, and E. S. Boss (2006), Climate-driven trends in contemporary ocean productivity, *Nature*, *444*(7120), 752–5, doi:10.1038/nature05317.
Bertilsson, S., O. Berglund, D. M. Karl, and S. W. Chisholm (2003), Elemental composition of marine Prochlorococcus and Synechococcus: Implications for the ecological stoichiometry of the sea, *Limnol. Oceanogr.*, *48*(5), 1721–1731, doi:10.4319/lo.2003.48.5.1721.
Bonjean, F., and G. S. E. Lagerloef (2002), Diagnostic model and analysis of the surface currents in the tropical Pacific Ocean, *J. Phys. Oceanogr.*, *32*(10), 2938–2954, doi:10.1175/1520-0485(2002)032<2938:DMAAOT>2.0.CO;2.
Box, G., and D. Cox (1964), An analysis of transformations, *J. R. Stat. Soc. Ser. B*, *26*(2), 211–252.
Boyce, D. G., M. R. Lewis, and B. Worm (2010), Global phytoplankton decline over the past century, *Nature*, *466*(7306), 591–6, doi:10.1038/nature09268.
Boyce, D. G., M. Lewis, and B. Worm (2012), Integrating global chlorophyll data from 1890 to 2010, *Limnol. Oceanogr. Methods*, *10*, 840–852, doi:10.4319/lom.2012.10.840.
Brainerd, K. E., and M. C. Gregg (1995), Surface mixed and mixing layer depths, *Deep Sea Res., Part I*, *42*(9), 1521–1543.
Brunet, C., and J. Lavaud (2010), Can the xanthophyll cycle help extract the essence of the microalgal functional response to a variable light environment?, *J. Plankton Res.*, *32*(12), 1609–1617, doi:10.1093/plankt/fbq104.
Burnham, K. P., and D. R. Anderson (2002), *Model Selection and Multi-Model Inference: A Practical Information-Theoretic Approach*, Springer, New York.
Casey, J. R., J. P. Aucan, S. R. Goldberg, and M. W. Lomas (2013), Changes in partitioning of carbon amongst photosynthetic pico- and nano-plankton groups in the Sargasso Sea in response to changes in the North Atlantic Oscillation, *Deep Sea Res., Part II*, *93*, 58–70, doi:10.1016/j.dsr2.2013.02.002.
Chatfield, C. (1975), *The Analysis of Time Series: Theory and Practice*, Chapman and Hall, London, U. K.
Cloern, J. E., C. Grenz, and L. Vidergar-Lucas (1995), An empirical model of the phytoplankton chlorophyll: Carbon ratio—The conversion factor between productivity and growth rate, *Limnol. Oceanogr.*, *40*(7), 1313–1321.
Corno, G., D. M. Karl, M. J. Church, R. M. Letelier, R. Lukas, R. R. Bidigare, and M. R. Abbott (2007), Impact of climate forcing on ecosystem processes in the North Pacific subtropical gyre, *J. Geophys. Res.*, *112*, C04021, doi:10.1029/2006JC003730.
Doran, H. E., W. E. Griffiths, and P. A. Beesley (1992), Further results on interval estimation in an AR(1) model, in *Readings in Econometric Theory and Practice*, edited by W. E. Griffiths, H. Lutkepohl, and M. E. Bock, pp. 175–194, Elsevier Science, Amsterdam, Netherlands.
DuRand, M. D., R. J. Olson, and S. W. Chisholm (2001), Phytoplankton population dynamics at the Bermuda Atlantic time-series station in the Sargasso Sea, *Deep Sea Res., Part II*, *48*(8–9), 1983–2003, doi:10.1016/S0967-0645(00)00166-1.
Fawcett, S., M. Lomas, B. Ward, and D. Sigman (2014), The counterintuitive effect of summer-to-fall mixed layer deepening on eukaryotic new production in the Sargasso Sea, *Global Biogeochem. Cycles*, *28*, 86–102, doi:10.1002/2013GB004579.
Follows, M., and S. Dutkiewicz (2002), Meteorological modulation of the North Atlantic spring bloom, *Deep Sea Res., Part II*, *49*, 321–344.
Frias-Lopez, J., A. Thompson, J. Waldbauer, and S. W. Chisholm (2009), Use of stable isotope-labelled cells to identify active grazers of picocyanobacteria in ocean surface waters, *Environ. Microbiol.*, *11*(2), 512–525, doi:10.1111/j.1462-2920.2008.01793.x.
Geider, R. J., H. L. MacIntyre, and T. M. Kana (1998), A dynamic regulatory model of phytoplanktonic temperature acclimation to light, nutrients, and temperature, *Limnol. Oceanogr.*, *43*(4), 679–694.
Glover, H. E., C. Garside, and C. C. Trees (2007), Physiological responses of Sargasso Sea picoplankton to nanomolar nitrate perturbations, *J. Plankton Res.*, *29*(3), 263–274, doi:10.1093/plankt/fbm013.
Graff, J. R., A. J. Milligan, and M. J. Behrenfeld (2012), The measurement of phytoplankton biomass using flow-cytometric sorting and elemental analysis of carbon, *Limnol. Oceanogr. Methods*, *10*, 910–920, doi:10.4319/lom.2012.10.910.
Hartmann, M., C. Grob, G. A. Tarran, A. P. Martin, P. H. Burkill, D. J. Scanlan, and M. V. Zubkov (2012), Mixotrophic basis of Atlantic oligotrophic ecosystems, *Proc. Natl. Acad. Sci. U.S.A.*, *109*(15), 5756–5760, doi:10.1073/pnas.1118179109.
Hastie, T., R. Tibshirani, and J. Friedman (2009), *The Elements of Statistical Learning: Data Mining, Inference, and Prediction*, 2nd ed., Springer, New York.
Henson, S. A., J. L. Sarmiento, J. P. Dunne, L. Bopp, I. Lima, S. C. Doney, J. John, and C. Beaulieu (2010), Detection of anthropogenic climate change in satellite records of ocean chlorophyll and productivity, *Biogeosciences*, *7*(2), 621–640, doi:10.5194/bg-7-621-2010.
Higgins, H. W., S. W. Wright, and L. Schluter (2011), Quantitative interpretation of chemotaxonomic pigment data, in *Phytoplankton Pigments: Characterization, Chemotaxonomy and Applications in Oceanography*, edited by S. Roy et al., pp. 257–313, Cambridge Univ. Press, Cambridge, U. K.
Hofmann, M., B. Worm, S. Rahmstorf, and H. J. Schellnhuber (2011), Declining ocean chlorophyll under unabated anthropogenic CO_2 emissions, *Environ. Res. Lett.*, *6*(3), 034035, doi:10.1088/1748-9326/6/3/034035.
Hurrell, J. W., and C. Deser (2009), North Atlantic climate variability: The role of the North Atlantic Oscillation, *J. Mar. Syst.*, *78*(1), 28–41, doi:10.1016/j.jmarsys.2008.11.026.
Karl, D. M., K. M. Bjorkman, J. E. Dore, L. Fujieki, D. V. Hebel, T. Houlihan, R. M. Letelier, L. M. Tupas, and K. M. Bjo (2001), Ecological nitrogen-to-phosphorus stoichiometry at station ALOHA, *Deep Sea Res., Part II*, *48*, 1529–1566.
Keller, K., et al. (2012), Variability of the ocean carbon cycle in response to the North Atlantic Oscillation, *Tellus B*, *1*, 1–25.
Krause, J. W., M. W. Lomas, and D. M. Nelson (2009), Biogenic silica at the Bermuda Atlantic Time-series Study site in the Sargasso Sea: Temporal changes and their inferred controls based on a 15-year record, *Global Biogeochem. Cycles*, *23*, GB3004, doi:10.1029/2008GB003236.
Kulk, G., W. H. Van de Poll, R. J. W. Visser, and A. G. J. Buma (2011), Distinct differences in photoacclimation potential between prokaryotic and eukaryotic oceanic phytoplankton, *J. Exp. Mar. Bio. Ecol.*, *398*(1–2), 63–72, doi:10.1016/j.jembe.2010.12.011.
Lessard, E. J., and M. C. Murrell (1998), Microzooplankton herbivory and phytoplankton growth in the northwestern Sargasso Sea, *Aquat. Microb. Ecol.*, *16*, 173–188.
Lipschultz, F. (2001), A time-series assessment of the nitrogen cycle at BATS, *Deep Sea Res., Part II*, *48*(8–9), 1897–1924, doi:10.1016/S0967-0645(00)00168-5.
Lipschultz, F., N. R. Bates, C. A. Carlson, and D. A. Hansell (2002), New production in the Sargasso Sea: History and current status, *Global Biogeochem. Cycles*, *16*(1), 1001, doi:10.1029/2000GB001319.
Lomas, M. W., and N. R. Bates (2004), Potential controls on interannual partitioning of organic carbon during the winter/spring phytoplankton bloom at the Bermuda Atlantic Time-series Study (BATS) site, *Deep Sea Res., Part I*, *51*(11), 1619–1636, doi:10.1016/j.dsr.2004.06.007.

Lomas, M. W., A. Swain, R. Shelton, and J. W. Ammerman (2004), Taxonomic variability of phosphorus stress in Sargasso Sea phytoplankton, *Limnol. Oceanogr.*, *49*(6), 2303–2310.
Lomas, M. W., N. Roberts, F. Lipschultz, J. W. Krause, D. M. Nelson, and N. R. Bates (2009), Biogeochemical responses to late-winter storms in the Sargasso Sea. IV. Rapid succession of major phytoplankton groups, *Deep Sea Res., Part I*, *56*(6), 892–908, doi:10.1016/j.dsr.2009.03.004.
Lomas, M. W., D. K. Steinberg, T. Dickey, C. A. Carlson, N. B. Nelson, R. H. Condon, and N. R. Bates (2010a), Increased ocean carbon export in the Sargasso Sea linked to climate variability is countered by its enhanced mesopelagic attenuation, *Biogeosciences*, *7*(1), 57–70, doi:10.5194/bg-7-57-2010.
Lomas, M. W., A. L. Burke, D. A. Lomas, D. W. Bell, C. Shen, S. T. Dyhrman, and J. W. Ammerman (2010b), Sargasso Sea phosphorus biogeochemistry: An important role for dissolved organic phosphorus (DOP), *Biogeosciences*, *7*(2), 695–710, doi:10.5194/bg-7-695-2010.
Lomas, M. W., N. R. Bates, R. J. Johnson, A. H. Knap, D. K. Steinberg, and C. A. Carlson (2013), Two decades and counting: 24-years of sustained open ocean biogeochemical measurements in the Sargasso Sea, *Deep Sea Res., Part II*, *93*, 16–32, doi:10.1016/j.dsr2.2013.01.008.
Lozier, M. S., A. C. Dave, J. B. Palter, L. M. Gerber, and R. T. Barber (2011), On the relationship between stratification and primary productivity in the North Atlantic, *Geophys. Res. Lett.*, *38*, L18609, doi:10.1029/2011GL049414.
Mahadevan, A., L. N. Thomas, and A. Tandon (2008), Comment on "Eddy/Wind Interactions Stimulate Extraordinary Mid-Ocean Plankton Blooms", *Science*, *320*, 448b, doi:10.1126/science.1152111.
Malmstrom, R. R., A. Coe, G. C. Kettler, A. C. Martiny, J. Frias-Lopez, E. R. Zinser, and S. W. Chisholm (2010), Temporal dynamics of Prochlorococcus ecotypes in the Atlantic and Pacific Oceans, *ISME J.*, *4*(10), 1252–1264, doi:10.1038/ismej.2010.60.
Malone, T. C., S. E. Pike, and D. J. Conley (1993), Transient variations in phytoplankton productivity at the JGOFS Bermuda time series station, *Deep Sea Res., Part I*, *40*(5), 903–924.
Mann, E. L., J. W. Moffett, W. Hole, and S. W. Chisholm (2002), Copper toxicity and cyanobacteria ecology in the Sargasso Sea, *Limnol. Oceanogr.*, *47*(4), 976–988.
Marra, J., R. R. Bigidare, and T. D. Dickey (1990), Nutrients and mixing, chlorophyll and phytoplankton growth, *Deep Sea Res., Part I*, *37*(1), 127–143.
Martinez, E., D. Antoine, F. D'Ortenzio, and B. Gentili (2009), Climate-driven basin-scale decadal oscillations of oceanic phytoplankton, *Science*, *326*(5957), 1253–6, doi:10.1126/science.1177012.
McGillicuddy, D. J., L. A. Anderson, S. C. Doney, and M. E. Maltrud (2003), Eddy-driven sources and sinks of nutrients in the upper ocean: Results from a 0.1° resolution model of the North Atlantic, *Global Biogeochem. Cycles*, *17*(2), 1035, doi:10.1029/2002GB001987.
McGillicuddy, D. J., et al. (2007), Eddy/wind interactions stimulate extraordinary mid-ocean plankton blooms, *Science*, *316*(5827), 1021–1026, doi:10.1126/science.1136256.
Mella-flores, D., et al. (2012), Prochlorococcus and Synechococcus have evolved different adaptive mechanisms to cope with light and UV stress, *Front. Microbiol.*, *3*, 1–20, doi:10.3389/fmicb.2012.00285.
Moisan, T. A. H., J. R. Moisan, M. A. Linkswiler, and R. A. Steinhardt (2013), Algorithm development for predicting biodiversity based on phytoplankton absorption, *Cont. Shelf Res.*, *55*, 17–28, doi:10.1016/j.csr.2012.12.011.
Mongin, M., D. M. Nelson, P. Pondaven, M. A. Brzezinski, and P. Tréguer (2003), Simulation of upper-ocean biogeochemistry with a flexible-composition phytoplankton model: C, N and Si cycling in the western Sargasso Sea, *Deep Sea Res., Part I*, *50*(12), 1445–1480, doi:10.1016/j.dsr.2003.08.003.
Montgomery, D. C., E. A. Peck, and G. G. Vining (2012), *Introduction to Linear Regression Analysis*, 5th ed., Wiley, New York.
Moore, C. M., M. M. Mills, R. Langlois, D. Kiel, A. Milne, E. P. Achterberg, J. La Roche, and R. J. Geider (2008), Relative influence of nitrogen and phosphorus availability on phytoplankton physiology and productivity in the oligotrophic sub-tropical North Atlantic Ocean, *Limnol. Oceanogr.*, *53*(1), 291–305.
Oschlies, A. (2001), NAO-induced long-term changes in nutrient supply to the surface waters of the North Atlantic, *Geophys. Res. Lett.*, *28*(9), 1751–1754, doi:10.1029/2000GL012328.
Oschlies, A. (2002), Can eddies make ocean deserts bloom?, *Global Biogeochem. Cycles*, *16*(4), 1106, doi:10.1029/2001GB001830.
Pan, X., A. Mannino, M. E. Russ, S. B. Hooker, and L. W. Harding (2010), Remote sensing of phytoplankton pigment distribution in the United States northeast coast, *Remote Sens. Environ.*, *114*(11), 2403–2416, doi:10.1016/j.rse.2010.05.015.
Parsons, R. J., M. Breitbart, M. W. Lomas, and C. A. Carlson (2012), Ocean time-series reveals recurring seasonal patterns of virioplankton dynamics in the northwestern Sargasso Sea, *ISME J.*, *6*(2), 273–284, doi:10.1038/ismej.2011.101.
Patara, L., M. Visbeck, S. Masina, G. Krahmann, and M. Vichi (2011), Marine biogeochemical responses to the North Atlantic Oscillation in a coupled climate model, *J. Geophys. Res.*, *116*, C07023, doi:10.1029/2010JC006785.
Polimene, L., C. Brunet, M. Butenschon, V. Martinez-Vicente, C. Widdicombe, R. Torres, and J. I. Allen (2013), Modelling a light-driven phytoplankton succession, *J. Plankton Res.*, *36*(1), 214–229, doi:10.1093/plankt/fbt086.
Polovina, J. J., E. A. Howell, and M. Abecassis (2008), Ocean's least productive waters are expanding, *Geophys. Res. Lett.*, *35*, L03618, doi:10.1029/2007GL031745.
Pyper, B. J., and R. M. Peterman (1998), Comparison of methods to account for autocorrelation in correlation analyses of fish data, *Can. J. Fish. Aquat. Sci.*, *55*(9), 2127–2140, doi:10.1139/cjfas-55-9-2127.
Roman, M. R., H. Dam, A. Gauzens, and J. Napp (1993), Zooplankton biomass and grazing at the JGOFS Sargasso Sea time series station, *Deep Sea Res., Part I*, *40*(5), 883–901, doi:10.1016/0967-0637(93)90079-I.
Saba, V. S., et al. (2010), Challenges of modeling depth-integrated marine primary productivity over multiple decades: A case study at BATS and HOT, *Global Biogeochem. Cycles*, *24*, GB3020, doi:10.1029/2009GB003655.
Sanders, R., U. Berninger, E. Lim, P. Kemp, and D. Caron (2000), Heterotrophic and mixotrophic nanoplankton predation on picoplankton in the Sargasso Sea and on Georges Bank, *Mar. Ecol. Prog. Ser.*, *192*, 103–118.
Sathyendranath, S., V. Stuart, T. Platt, H. Bouman, O. Ulloa, and H. Maass (2005), Remote sensing of ocean colour: Towards algorithms for retrieval of pigment composition, *Indian J. Mar. Sci.*, *34*(4), 333–340.
Schnetzer, A., and D. K. Steinberg (2002), Natural diets of vertically migrating zooplankton in the Sargasso Sea, *Mar. Biol.*, *141*(1), 89–99, doi:10.1007/s00227-002-0815-8.
Siegel, D., et al. (2001), Bio-optical modeling of primary production on regional scales: The Bermuda BioOptics project, *Deep Sea Res., Part II*, *48*(8–9), 1865–1896, doi:10.1016/S0967-0645(00)00167-3.
Siegel, D. A., D. J. McGillicuddy, and E. A. Fields (1999), Mesoscale eddies, satellite altimetry, and new production in the Sargasso Sea, *J. Geophys. Res.*, *104*, 359–380.
Six, C., Z. V. Finkel, A. J. Irwin, and D. A. Campbell (2007), Light variability illuminates niche-partitioning among marine Picocyanobacteria, *PLoS One*, *2*(12), e1341, doi:10.1371/journal.pone.0001341.

Sprintall, J., and M. Tomczak (1992), Evidence of the barrier layer in the surface layer of the tropics, *J. Geophys. Res.*, *97*(C5), 7305–7316, doi:10.1029/92JC00407.

Steinacher, M., et al. (2010), Projected 21st century decrease in marine productivity: A multi-model analysis, *Biogeosciences*, *7*, 979–1005.

Steinberg, D. K., C. A. Carlson, N. R. Bates, R. J. Johnson, A. F. Michaels, and A. H. Knap (2001), Overview of the US JGOFS Bermuda Atlantic Time-series Study (BATS): A decade-scale look at ocean biology and biogeochemistry, *Deep Sea Res., Part II*, *48*(8–9), 1405–1447, doi:10.1016/S0967-0645(00)00148-X.

Steinberg, D. K., M. W. Lomas, and J. S. Cope (2012), Long-term increase in mesozooplankton biomass in the Sargasso Sea: Linkage to climate and implications for food web dynamics and biogeochemical cycling, *Global Biogeochem. Cycles*, *26*, GB1004, doi:10.1029/2010GB004026.

Stow, C. A., J. Jolliff, D. J. McGillicuddy, S. C. Doney, J. I. Allen, M. A. M. Friedrichs, K. A. Rose, and P. Wallhead (2009), Skill assessment for coupled biological/physical models of marine systems, *J. Mar. Syst.*, *76*(1–2), 4–15, doi:10.1016/j.jmarsys.2008.03.011.

Taylor, G. T., et al. (2012), Ecosystem responses in the southern Caribbean Sea to global climate change, *Proc. Natl. Acad. Sci. U.S.A.*, *109*(47), 19,315–19,320, doi:10.1073/pnas.1207514109.

Veldhuis, M. J. W., and G. W. Kraay (2000), Application of flow cytometry in marine phytoplankton research: Current applications and future perspectives, *Sci. Mar.*, *64*(2), 121–134.

Veldhuis, M. J. W., and G. W. Kraay (2004), Phytoplankton in the subtropical Atlantic Ocean: Towards a better assessment of biomass and composition, *Deep Sea Res., Part I*, *51*(4), 507–530, doi:10.1016/j.dsr.2003.12.002.

Westberry, T., M. J. Behrenfeld, D. A. Siegel, and E. Boss (2008), Carbon-based primary productivity modeling with vertically resolved photoacclimation, *Global Biogeochem. Cycles*, *22*, GB2024, doi:10.1029/2007GB003078.

Worden, A., and B. Binder (2003), Application of dilution experiments for measuring growth and mortality rates among Prochlorococcus and Synechococcus populations in oligotrophic environments, *Aquat. Microb. Ecol.*, *30*, 159–174, doi:10.3354/ame030159.

Worden, A. Z., G. Drive, L. Jolla, and J. K. Nolan (2004), Assessing the dynamics and ecology of marine picophytoplankton: The importance of the eukaryotic component, *Limnol. Oceanogr.*, *49*(1), 168–179.

Yool, A., E. E. Popova, A. C. Coward, D. Bernie, and T. R. Anderson (2013), Climate change and ocean acidification impacts on lower trophic levels and the export of organic carbon to the deep ocean, *Biogeosciences*, *10*(9), 5831–5854, doi:10.5194/bg-10-5831-2013.